Kinetics of cluster-related defects in silicon sensors irradiated with monoenergetic electrons

R. Radu,[1] I. Pintilie,[1,a)] L. F. Makarenko,[2] E. Fretwurst,[3] and G. Lindstroem[3]
[1]*National Institute of Materials Physics, Atomistilor 105 bis, Magurele 077125, Romania*
[2]*Belarusian State University, Independence Ave. 4, 220030 Minsk, Belarus*
[3]*Institute for Experimental Physics, University of Hamburg, D-22761 Hamburg, Germany*

(Received 31 October 2017; accepted 6 February 2018; published online 28 February 2018)

This work focuses on the kinetic mechanisms responsible for the annealing behavior of radiation cluster-related defects with impact on the electrical performance of silicon sensors. Such sensors were manufactured on high resistivity n-type standard float-zone (STFZ) and oxygen enriched float-zone (DOFZ) material and had been irradiated with mono-energetic electrons of 3.5 MeV energy and fluences of $3 \times 10^{14}\,cm^{-2}$ and $6 \times 10^{14}\,cm^{-2}$. After irradiation, the samples were subjected either to isochronal or isothermal heat treatments in the temperature range from 80 °C to 300 °C. The specific investigated defects are a group of three deep acceptors [H(116 K), H(140 K), and H(152 K)] with energy levels in the lower half of the band gap and a shallow donor E(30 K) with a level at 0.1 eV below the conduction band. The stability and kinetics of these defects at high temperatures are discussed on the basis of the extracted activation energies and frequency factors. The annealing of the H defects takes place similarly in both types of materials, suggesting a migration rather than a dissociation mechanism. On the contrary, the E(30 K) defect shows a very different annealing behavior, being stable in STFZ even at 300 °C, but annealing-out quickly in DOFZ material at temperatures higher than 200 °C , with a high frequency factor of the order of $10^{13}\,s^{-1}$. Such a behavior rules out a dissociation process, and the different annealing behavior is suggested to be related to a bistable behavior of the defect. *Published by AIP Publishing.*
https://doi.org/10.1063/1.5011372

I. INTRODUCTION

Over the last three decades, considerable effort has been put into understanding the underlying mechanisms of radiation damage in silicon, pad,[1–20] and segmented sensors (i.e., micro-strips and pixels devices)[21–24] and correlating the effects observed at the microscopic level with the electrical performance of irradiated silicon devices.[10–20] Many of these studies have been mainly driven by the need for developing devices for charged particle tracking at the Large Hadron Collider (LHC) and its upgrade, the High-Luminosity LHC.[25,26] The unique features of the environment where silicon tracking detectors perform[27] require extensive knowledge of radiation effects to assess the performance degradation of particle detectors induced by radiation damage. This paper presents a rigorous study of the damage generated by electron irradiation in silicon for applications in high energy physics, emphasizing the mechanisms for the disappearance of clusters at high temperature. It should be mentioned that in the innermost area of the High-Luminosity LHC experiments, where the radiation challenge is most severe, charged hadrons (mainly pions) prevail, and thus, a mixture of point and cluster effects is generated.[13,28] This makes it extremely difficult to correlate the results of defect analysis methods with the consequences to be seen in the degradation of the detector performance. Conclusive results would only be possible if point defect and cluster effects could be much better separated. In this respect, we have chosen irradiation with electrons of low energy (3.5 MeV), where, as we will show further, the generation of extended defects starts to affect the device performance and the separation between point and extended defects can be resolved.

The effects of radiation damage upon silicon tracking devices can be summarized in two classes: bulk damage and surface damage. The former is due to the Non-Ionizing Energy Loss (NIEL) of incident particles (i.e., protons, neutrons, electrons and gamma-rays), leading to a permanent damage of the silicon crystal structure, whilst the latter is due to the ionizing energy loss of charged particles or X-ray photons, generating positive charges and traps in the SiO_2 and at the Si-SiO_2 interface.[29] This paper deals with the damage effects induced by irradiation in the bulk of the silicon sensors. In this context, during the last three decades, great progress has been made on the detection and characterization of the bulk defects with strong consequences on the electrical properties of silicon sensors at room temperature, their annealing behavior with time and temperature, energy, and fluence dependence as well as their bi-stability.[1–20]

The detailed work presented in this paper has been largely motivated by a lack of information available regarding the nature (i.e., chemical structure) of the main cluster-related defects, the H defects, and the E(30 K) donor, with a strong impact on the effective doping concentration (N_{eff}) after irradiation. It has been experimentally shown that the E(30 K)—a shallow donor in the upper part of the silicon band gap—is contributing to the "short-term" beneficial

a)Author to whom correspondence should be addressed: ioana@infim.ro

annealing after hadron irradiation,[13] whereas the H(116 K), H(140 K), and H(152 K)—deep acceptors in the lower part of the gap—are cluster-related hole traps with enhanced field emission, fully contributing with their concentration to N_{eff} and causing long term reverse annealing in the hadron irradiated silicon diodes.[13,17] A significant improvement of the silicon material in regards to radiation hardness can only be achieved by a thorough knowledge of the kinetics (generation and annealing) of cluster-related defects in the bulk material.

It should be emphasized that a combined study, correlating the data obtained by Electron Spin Resonance (ESR), often called Electron Paramagnetic Resonance (EPR), in terms of paramagnetic centers, with those from Deep Level Transient Spectroscopy (DLTS) and Thermally Stimulated Current (TSC) techniques, in terms of electrically active defects, would provide a complete picture of cluster related defects. Based on this, one can significantly improve sensor performance based on defect engineering processes. However, the main difficulty in correlating the results obtained by these different techniques is related to the sensitivities with respect to the defect concentrations needed for each of the mentioned techniques. Thus, on samples similar to those investigated in this work, the DLTS is only applicable for defect concentrations of a few percent of the doping concentration, the TSC technique can go up to defect concentrations of $10^{13}\,cm^{-3}$, the limitation being ultimately the magnitude of the reverse bias to be applied for fully depleting the diodes, and the ESR requires defect concentration above $10^{17}\,cm^{-3}$. In addition, the majority of the studies relating ESR/EPR in silicon irradiated were performed between the 60s and 80s with either neutrons or electrons,[30–34] and no recent or conclusive data can be found that can correlate the extended defects studied here with specific chemical defect structures. Within this context, the investigations reported here are intended to bring new insights into the annealing kinetics of cluster-induced defects, with a direct impact on the performance of the Si-based sensors.

II. EXPERIMENTAL DETAILS

A. Samples and irradiation

The n-type silicon detectors, crystal orientation of ⟨100⟩ and thickness 280 μm were fabricated by CiS[35] using standard silicon planar processing technology. All the diodes have an active area of $5 \times 5\,mm^2$ surrounded by a p^+ guard ring, grounded for all the performed electrical measurements to exclude the contribution of surface currents to the measured signal. It should be mentioned that the pad diodes are simple planar diodes without segmentation with a simple geometry (well-defined sensor volume, a high electrical strength and a simple electrical field distribution), which makes them appropriate for quantitative defect analysis. Detailed information regarding the features of the diodes can be found in Ref. 10. For the investigation of the cluster defects a total of 12 silicon detectors, of n-type standard float-zone (STFZ) and oxygen enriched float-zone (DOFZ) materials, were irradiated with mono-energetic electrons of 3.5 MeV, and fluence value of $3 \times 10^{14}\,cm^{-2}$ and $6 \times 10^{14}\,cm^{-2}$, at the Belarusian State University.[36] The main impurities existing in the samples were determined by Secondary Ion Mass Spectroscopy.[37] These measurements have shown that although the Carbon content is the same, $2 \times 10^{15}\,cm^{-3}$ in the two types of materials, the Oxygen concentration in the bulk is $<5 \times 10^{15}\,cm^{-3}$ in STFZ and in average $1.2 \times 10^{17}\,cm^{-3}$ in DOFZ.[13]

B. Characterization

The investigations on electron-induced cluster defects have been performed using the TSC technique with the guard ring grounded for assuring accurate trap concentration values.[38] The typical TSC procedure used in this work consists of filling the defects at low temperature (T = 10 K), by applying a forward current of 2 mA for 30 s, followed by heating-up under reverse bias with a constant rate 0.183 K/s.

For a complete picture of the evolution of the defects with the temperature, isochronal annealing for 30 min in steps of 20 °C from 80 °C up to 300 °C was performed. Furthermore, to determine the key mechanisms involved in the kinetics of the annealing-out, isothermal annealing studies have been carried out at temperatures higher than 200 °C. This study is performed with the aim of identifying the mechanisms leading to the disappearance/reduction of cluster-related defects responsible for the deterioration of Si sensors, namely, the E(30 K) and H defects.

C. Defect kinetics

There are three basic mechanisms governing defect annealing: migration, complex formation, and dissociation processes.[39] Defects become mobile at specific temperatures at which the thermal energy accelerates the process of annealing and their concentration drops below the (1/e)-th part in a certain time interval, labeled annealing temperature (T_{ann}). The general expression for the reaction kinetics of a defect that anneals out is given by

$$-\frac{dN_x}{dt} = k_\gamma N_x{}^\gamma, \tag{1}$$

where N_x is the defect concentration and $k = k_0 \exp\left(-\frac{E_a}{k_B T}\right)$ is the rate constant; k_0 and E_a are the frequency factor and the activation energy, respectively, specific for each of the three mechanisms mentioned above. The frequency factor is related to the attempt-to-escape frequency that can be estimated by the most abundant phonon frequency $\left[\approx \frac{k_B T}{h} = 2.1 \times 10^{10} * T(K) s^{-1}\right]$. The γ parameter stands for the order of the reaction. Thus, for a first and second order reaction, the time dependence of N_x is given by

$$\begin{aligned} \gamma = 1: &\quad N_x(t) = N_x|_{t=0} \exp(-k_1 t), \\ \gamma = 2: &\quad N_x(t) = N_x|_{t=0} \frac{1}{1 + k_2 N_x|_{t=0} t}. \end{aligned} \tag{2}$$

III. EXPERIMENTAL RESULTS

To understand the mechanisms leading to annealing of the envisaged cluster defects [E(30 K) and H type defects],

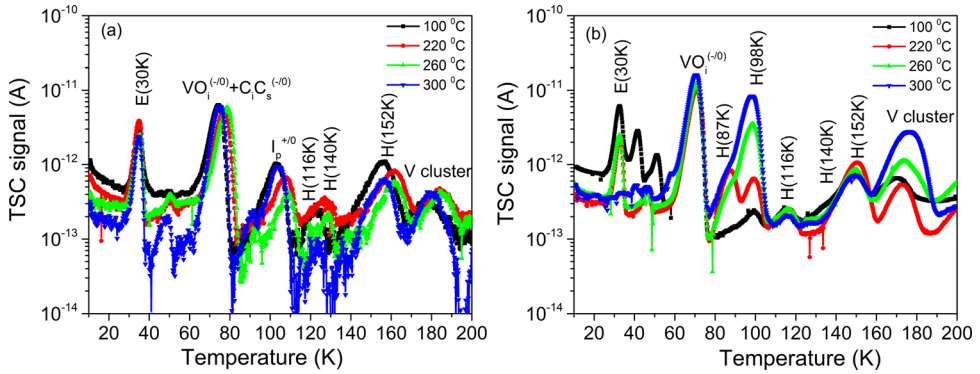

FIG. 1. TSC spectra measured on fully depleted (a) STFZ and (b) DOFZ diodes, irradiated with 3.5-MeV electrons and fluence of 3×10^{14} cm^{-2}. The silicon sensors were kept at each temperature for $t = 30$ min, and the temperature interval between two annealing points was $\Delta T = 20$ °C.

isochronal studies were first performed on STFZ and DOFZ silicon sensors in the temperature range 80 °C–300 °C. This procedure provides the advantage of examining the annealing processes that occur in silicon sensors, especially at high temperature conditions where these defects might undergo a transformation. A comparison of the TSC spectra recorded for STFZ and DOFZ sensors is illustrated in Fig. 1. The full depletion condition for all the annealing stages was achieved by applying a reverse bias of 200 V for STFZ and 300 V for DOFZ during the TSC temperature scans. The higher reverse bias needed to fully deplete the DOFZ diodes was required by the large amount of positive charge trapped on the H(98 K) center, in a concentration of 7×10^{11} cm^{-3} after the last step of annealing, similar to the initial doping concentration.

It has been shown previously that the process of generation and/or the annealing at temperatures close to ambient ones (≤80 °C) of E(30 K) and H type cluster related-defects depend on the oxygen content in the samples.[10] Based on the correspondence with the electrical properties of the irradiated silicon devices and on the dependence of defect generation on the impurity content in silicon (carbon and oxygen), significant hints concerning the chemical structure of these defects have been made. Suggested assignments of the above mentioned cluster-related defects are presented below:

(i) The E(30 K) cluster-related defect was found earlier to be generated more in DOFZ than in STFZ irradiated silicon[10] [compare also Fig. 1(a) with Fig. 1(b)] and was associated at some point with the donor state of the tri-interstitial $I_3^{(0/+)}$.[40] Moreover, by comparing the introduction rates between Czochralski and Float-Zone silicon, it was assumed that the E(30 K) defect can be associated with the interstitial-oxygen complex.[41] As seen in Fig. 1, the concentration of E(30 K) remains almost constant in STFZ during the isochronal thermal treatment up to 300 °C, whereas it decreases in DOFZ starting with the annealing at 200 °C. The disappearance from the TSC spectrum of the E(30 K) peak in DOFZ could not be connected with the increase of any other new signal [e.g., H(98 K) or V cluster in Fig. 1(b)].

(ii) The generation of the H defects takes place independently of oxygen concentration in STFZ and DOFZ silicon, leading to the conclusion that they are intrinsic defects. Moreover, they possess bi-stability at room temperature,[10] similar to the one observed for the tri-vacancies (V_3) and predicted for small vacancy clusters V_4 and V_5.[42] Based on these features, it was suggested that the H defects can be related to complexes of multi-vacancies (V_4, V_5).[10] It should be emphasized also that the high resolution transmission electron microscopy investigations showed that the clusters of vacancies and interstitials show similar contrast and distribution along the principal crystallographic directions, in DOFZ and STFZ materials, with an eventual dependence on the oxygen content in the samples being not observed.[10]

A. Annealing of the deep acceptors (H-defects)

According to the results of the annealing treatments shown in Fig. 2, the concentration of the H(116 K), H(140 K), and H(152 K), called in the following the H-defects, first increases with temperature up to temperatures above 200 °C. Such a process takes place also at ambient temperatures, and treatment lasts longer than 10.000 min. at 80 °C to reach the saturation.[10] This annealing-in process is followed by a progressive reduction of defect concentration

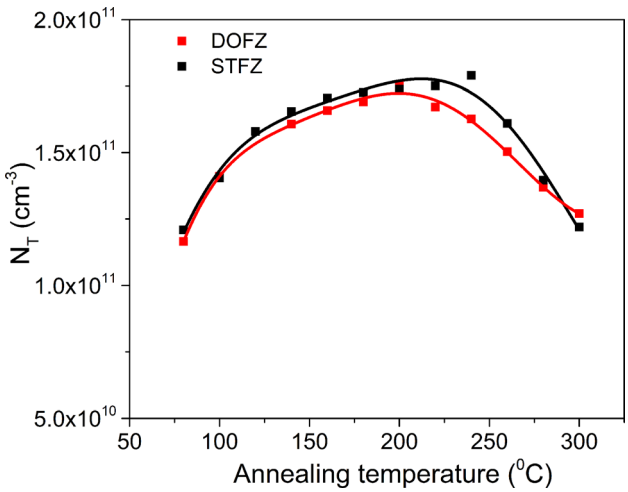

FIG. 2. Concentration of the sum of the H(116 K) + H(140 K) + H(152 K) defects in STFZ (black symbols) and DOFZ (red symbols) extracted from TSC spectra as a function of the annealing temperature. The diodes were irradiated with a fluence of 3×10^{14} cm^{-2}.

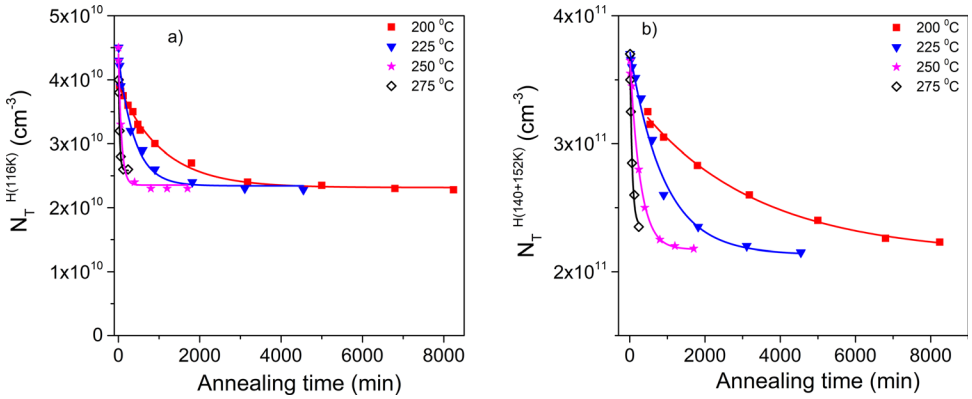

FIG. 3. Isothermal annealing, in STFZ, for (a) H(116 K) and (b) H(140 + 152 K) at different temperatures. The diodes were irradiated with a fluence of $6 \times 10^{14}\,\mathrm{cm}^{-2}$.

by increasing the temperature above 200 °C, in both STFZ and DOFZ materials. However, the temperatures at which the H defects start to anneal-out are slightly different: 220 °C in DOFZ and 260 °C in STFZ, indicating that the mechanisms for the annealing-out of cluster defects might be connected with the oxygen concentration. Oxygen is always present in a not negligible concentration in float-zone silicon sensors ($\leq 10^{16}\,\mathrm{cm}^{-3}$)—if no oxygen enrichment is considered—and is known to be a very efficient trap (sink) for migrating vacancies. The concentration of oxygen in DOFZ material was $1.2 \times 10^{17}\,\mathrm{cm}^{-3}$, whereas in STFZ, it is of the order of $10^{15}\,\mathrm{cm}^{-3}$. The obtained results reveal that upon isochronal annealing, a transformation of the H defects into other not electrically active centers might occur in the two Si materials. One has to mention that these defects do not anneal-out completely at 300 °C. According to the literature,[43] the small vacancy clusters V_3–V_6 anneal out at temperatures >300 °C.

To investigate the mechanisms leading to the decrease in concentration of the H-defects, isothermal annealing studies have been performed at five temperatures ranging from 200 °C to 290 °C. As mentioned above, the mechanisms leading to the annealing-out of defects are migration, formation, or dissociation processes. The main features of these processes reside in their activation energies and frequency factors.

The procedure we employed to determine the activation energy and the frequency factor is the following: 12 silicon sensors of STFZ and DOFZ materials were irradiated with electrons of 3.5 MeV energy and the same fluence value of $6 \times 10^{14}\mathrm{cm}^{-2}$ and further subjected to isothermal treatments at 200 °C, 225 °C, 250 °C, 275 °C, and 290 °C up to 8000 min (the time in which defects decrease in concentration). The values of the H defect concentrations were extracted from the corresponding TSC spectra (not shown here). The annealing of the STFZ and DOFZ samples at temperature ≥200 °C results in a progressive reduction in the concentration of H defects. The data were fitted with an exponential function and an offset [Eq. (2)] corresponding to a first order process. It should be mentioned that for both materials, the fit with a first order process was performed with a constant offset, implying that the annealing out of the H defects is a more complex process, with half of the defects remaining stable during the annealing experiments.

The temperature dependent time constants determined from these fits were used to build-up the Arrhenius plots according to $\frac{1}{\tau} = k_0 \exp\left(-\frac{E_a}{k_B T}\right)$. For a single rate-limited thermally activated process, the Arrhenius plot is a straight line from which the activation energy and the frequency factor can both be determined. The annealing behavior of the H(116 K) and sum of H(140 K + 152 K) and their fits are plotted in Figs. 3 and 4 for STFZ and DOFZ, respectively. The time constants extracted from these fits, summarized in Table I, were used to draw the Arrhenius plots in Fig. 5.

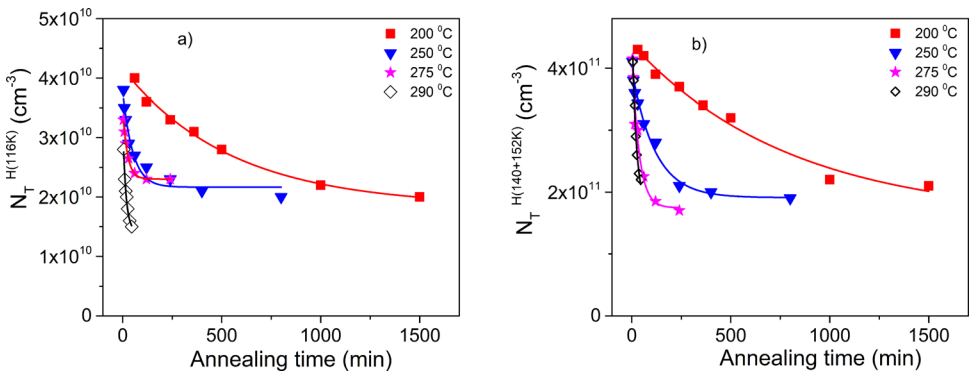

FIG. 4. Isothermal annealing, in DOFZ, for (a) H(116 K) and (b) H(140 + 152 K) at different temperatures. The diodes were irradiated with a fluence of $6 \times 10^{14}\,\mathrm{cm}^{-2}$.

TABLE I. Time constant for annealing-out of the H defects in STFZ and DOFZ materials irradiated with a fluence of 6×10^{14} cm^{-2}.

	$\tau_{H(116\,K)}$ (min)		$\tau_{H(140\,K+152\,K)}$ (min)	
Annealing temperature (°C)	DOFZ	STFZ	DOFZ	STFZ
200	551 ± 80	1070 ± 70	856 ± 130	3152 ± 365
225	…	393 ± 55	…	723 ± 141
250	51 ± 12	74 ± 11	111 ± 30	273 ± 19
275	23 ± 2	27 ± 3	35 ± 8	56 ± 7
290	15 ± 2	…	21 ± 3	…

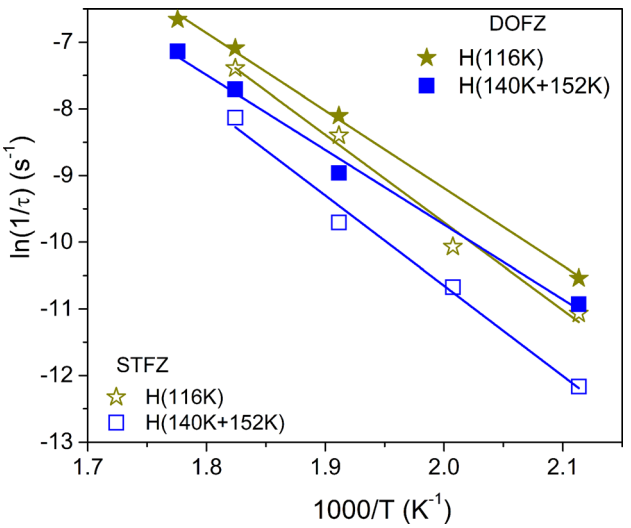

FIG. 5. Arrhenius plot of the rate constant for annealing-out of H(116 K) and H(140 + 152 K) in STFZ (open symbols) and DOFZ (filled symbols) materials.

Thus, Table I shows the time constants, τ, calculated for the decrease in the H-defects concentration in STFZ and DOFZ sensors corresponding to five distinct temperatures. As it can be seen, the τ values are significantly higher for STFZ than those for the DOFZ samples.

The corresponding Arrhenius plot using $\ln(1/\tau)$ versus 1000/T gives a straight line. From the slope of the line, the activation energy was deduced, whereas from the intercept, the frequency factor for processes involving the decrease of the H defect concentrations in STFZ and DOFZ materials was deduced. The values of these parameters, critical for understanding thermal activation processes, are displayed in Table II. The identification of the mechanisms leading to the annealing-out of the H defects is quite challenging as well as the most likely candidates for these processes. There are no details on experiments regarding the kinetics of cluster defects reported in the literature, and at this stage, these studies can only provide what appears to be the most probable reasons for defect transformations during the considered thermal treatments.

TABLE II. Activation energy and the frequency factor for the annealing-out of the H defects in STFZ and DOFZ materials.

	E_a (eV)		k_0 (s^{-1})	
Defect type	DOFZ	STFZ	DOFZ	STFZ
H(116 K)	0.99 ± 0.1	1.01 ± 0.1	10^8–10^9	10^6–10^8
H(140 K + 152 K)	1.01 ± 0.05	1.01 ± 0.1	10^7–10^9	10^7–10^8

One interpretation is that the Arrhenius plots in Fig. 5 show one step in the annealing-out process for both H(116 K) and H(140 + 152 K) defects, suggesting that only one mechanism is responsible for the annealing-out for both the H(116 K) and H(140 + 152 K) defects. The activation energies and frequency factors are of the order of 1.0 ± 0.1 eV and between 10^6 and 10^9 s^{-1}, respectively (see Table II).

However, because the loss in the H defect concentration is not substantial during the annealing at different temperatures, a second order process also fits the experimental data from Figs. 3 and 4. An example is given in Fig. 6. Considering a second order process, the largest activation energy resulted from Arrhenius plots is of ∼1.35 ± 0.1 eV and is common for both DOFZ and STFZ diodes. According to Ref. 6, to really distinguish between a first and second order process, one should analyze samples with different defect concentrations, which is a study that needs to be done in the near future.

It is known that the activation energy for migration processes is smaller than the activation energy for complex formation, which is smaller compared to activation energy for dissociation ($E_m \ll E_f \ll E_d$). This implies that if the cluster-related defects decrease in concentration due to a migration process, they will need a smaller energy to jump from an equilibrium position to another compared to a dissociation process, where the energy should be significantly higher if the clusters break-up into separate defects. Thus, from the three mechanisms of annealing-out, a dissociation process of the H defects can be ruled out as the frequency factors obtained for the two defects are in the 10^6–10^9 s^{-1} range, which is a factor of 10^4 up to 10^7 lower than expected if dissociation prevails (10^{12}–10^{13} s^{-1}). Furthermore, as stated above, the decrease of the H defects implies processes, of first or second order, involving long distance defect

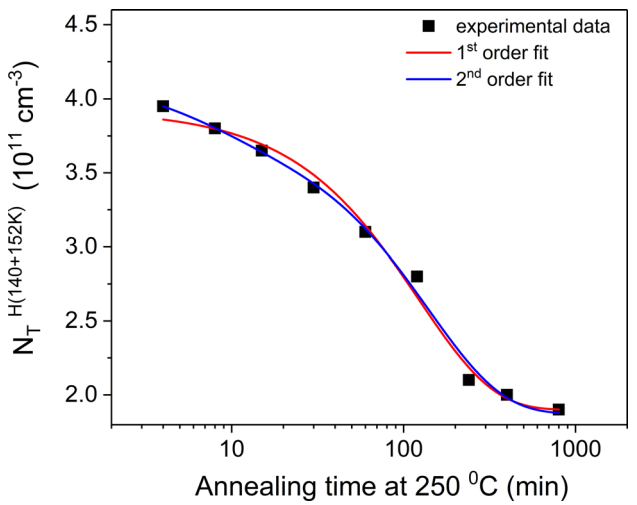

FIG. 6. Comparison of the first and second order fit for the H(140 + 152 K) defects. The experimental data represent the concentration of the H(140 + 152 K) defects extracted after isothermal annealing at 250 °C of a DOFZ diode irradiated with 3.5 MeV and fluence of 6×10^{14} cm^{-2}.

migration with subsequent trapping. Thus, the data presented here leads to the suggestion that the pathway by which the H(116 K) and H(140 + 152 K) defects anneal-out is their migration at temperatures above 200 °C and interaction with other defects/impurities in the material. However, in this study, no correlation could be made between the loss of H defects and the growth of any other electrically active center. We suggested earlier that the H defects can be associated with the formation of the small vacancy clusters V_4, V_5, and V_6 based mainly on their experimentally observed bi-stable behavior[10] that was also theoretically predicted.[42] Their annealing-out at temperatures above 200 °C is also in agreement with such assignments. However, the activation energy for the annealing-out process (∼1 eV for a first order process and 1.35 eV for the largest energy in a second order process) is lower than one would expect for vacancy clusters larger than V_2 where the migration occurs with an activation energy of 1.3 eV.[44] In this respect, the annealing-out of the H defects via a second order process seems more probable, and further studies need to be performed for identifying the mechanisms behind the annealing process of the H defects and their structure.

The annealing-out process is faster in DOFZ than in STFZ material. The only difference between the two types of sample materials is the concentration of oxygen that is more than 20 times higher in DOFZ than in STFZ. As is already known, the oxygen efficiently reacts with single vacancies or small vacancy clusters (V_2 and V_3) leading to electrically active vacancy-oxygen defects, V_2O and V_3O, with energy levels close to those of the migrating V_2 and V_3.[2,45] The single negatively charged acceptor states of V_2O and V_3O defects are expected to give a TSC signal in the temperature range close to 180 K, depicted in Fig. 1(b) as the V and O related-cluster peak. The signal labelled H(98 K) is attributed to the single positively charged donor state of the V_2O and V_3O defect, which exhibits nearly the same ionization energy of $E_V + 0.235$ eV.[46] Their formation is only detected in DOFZ material due to the significantly larger oxygen concentration in this material compared to STFZ Si (at least 20 times higher than in STFZ). Thus, it is reasonable to presume that oxygen can react also with slightly larger migrating vacancy clusters like V_4, V_5, or even V_6 according to Estreicher,[47] this being one of the possible pathways by which such vacancy clusters anneal-out and transform at these temperatures.

B. Annealing out of the E(30 K) donors

The E(30 K) donor was subjected to a similar isothermal procedure as for the H defects, being a first attempt to reveal information on its kinetics. This defect also has a significant influence on the space charge concentration, being a donor in the upper part of the silicon band-gap. The raw data regarding the concentration of E(30 K) versus annealing temperature are shown in Fig. 7(a) for STFZ and DOFZ materials. The results are surprising at first sight because this defect completely anneals out, in DOFZ material, at 300 °C, whereas in the STFZ diode, it has an almost constant concentration, with only a small increase, around 10% in the high temperature range. It should be mentioned that the E(30 K) defect is not detected directly after irradiation, in either of the two materials, but anneals-in after irradiation is stopped, reaching its maximum concentration after 200 min of annealing at 80 °C.[10] Worth noting is that the decrease in the E(30 K) defect concentration in DOFZ is directly observed in the change of N_{eff}, as shown in Fig. 7(b). Thus, in STFZ, E(30 K) stays almost constant for temperatures above 200 °C, and only the H defects anneal out [seen as a recover of N_{eff} in Fig. 7(b)], whereas in DOFZ, the decay in E(30 K) concentration is also reflected in a decay of N_{eff}.

The obtained data show that only in DOFZ material does annealing above 200 °C result in a progressive reduction in the concentration of the E(30 K) defect. Information about the activation energy and the frequency factor can be extracted if the annealing is performed at more than two different temperatures. Thus, isothermal annealing experiments were performed on DOFZ samples irradiated with a 3.5-MeV electron and fluence of $6 \times 10^{14}\text{cm}^{-2}$ at three distinct temperatures: 225 °C, 275 °C, and 290 °C [Fig. 8(a)].

The obtained annealing time constants were used to calculate the activation energy and the frequency factor for the annealing-out process [see Fig. 8(b)]. Similar to the H defects, the Arrhenius plot of $\ln(1/\tau)$ versus 1000/T gives a straight line. Thus, the decrease of the E(30 K) defect exhibits a first-order process. The activation energy and the frequency factor for the annealing-out of the E(30 K) are $E_a = 1.8 \pm 0.1$ and $k_0 \approx 2 \times 10^{13}\ \text{s}^{-1}$.

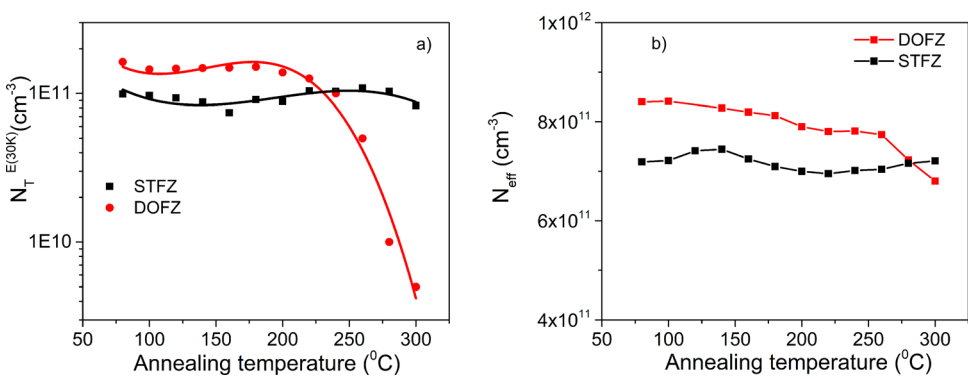

FIG. 7. (a) Isochronal annealing development of the E(30 K) defect in STFZ and DOFZ silicon material. Measurements were done on diodes irradiated with 3.5 MeV and a fluence of $\Phi = 3 \times 10^{14}\text{cm}^{-2}$; (b) change in the N_{eff} as determined from monitoring the capacitance-voltage characteristics at 10 kHz.

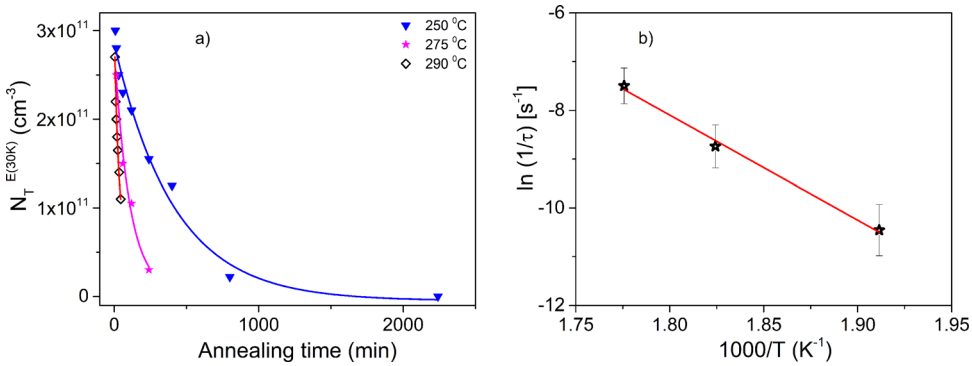

FIG. 8. Annealing out of the E(30 K) defect in DOFZ material irradiated with a fluence of 6×10^{14} cm^{-2}. (a) Isothermal annealing, at different temperatures. (b) Arrhenius plot corresponding to the annealing-out of E(30 K).

Initially, with a first order kinetics and a frequency factor k_0 close to the most abundant phonon frequency, the annealing of the E(30 K) defect seems to be due to the dissociation process. However, because the defect is still stable in STFZ material, a dissociation mechanism cannot be the cause for the behavior observed in DOFZ. In the absence of dissociation, such a high frequency factor can be explained, in our opinion, considering that the E(30 K) also has a bi-stable behavior, as do most of the detected cluster-related defects [earlier thermal double donors TDD1 and TDD2, V_3, H(116 K), and H(140 + 152 K) defects]. Compared with the STFZ case, one can observe from Fig. 1 that in DOFZ, the high oxygen content leads to the formation of more defects than in STFZ during the heat treatment. The presence of these defects surely changes the position of the Fermi level, and this way, the charging of a bistable defect can be affected. We do not yet have detailed experimental studies on this matter, and further work is needed. Correlated fundamental studies with structure sensitive methods (e.g., Infrared Absorption and EPR) should be considered to clarify the chemical identity of the observed cluster-related defect. However, we studied the bi-stability of the E(30 K) defect as seen in the TSC signal measured on a similar irradiated STFZ sample subjected to different conditions of excitation with thermal treatment at 80 °C. The results are shown in Fig. 9. One can observe that the largest signal from E(30 K) is measured immediately after the heat treatment. By keeping the sample in the dark, the signal decrease and an injection with a current density of 4 A/cm^2 at ambient temperatures restores part of the initial signal. Similar effects were previously observed on other bistable defects as V_3, H defects, and a bi-stable donor (BD) induced by irradiation associated with the earlier thermal donors TDD2.[16,18,48] It is important to mention that the disappearance of the E(30 K) defect could not be connected with the formation of other electrical active defects, with the loss of the E(30 K) signal being fully observed in the change of N_{eff}, shown in Fig. 7(b). Accounting for all of the defects detected by TSC that are influencing the N_{eff} at room temperature [BD, E(30 K), I_p, H(116 K), and H(140 + 152 K) defects], a good agreement is obtained with the values obtained from C-V measurements performed at 20 °C. Figure 10 gives some examples in the case of both STFZ and DOFZ diodes, irradiated with 6×10^{14} cm^{-2} during isothermal annealing at 250 °C [Figs. 10(a) and 10(b)].

IV. CONCLUSIONS

Using isothermal annealing at temperatures above 200 °C on DOFZ and STFZ silicon detectors irradiated with 3.5-MeV electrons and fluences of 3×10^{14} cm^{-2} and 6×10^{14} cm^{-2}, we have determined the activation energies and the frequency factors for the mechanisms of annealing-out of irradiation induced trapping centers, the acceptors H(116 K) and H(140 + 152 K) defects, and the donor E(30 K).

It was found that, for the experiments performed here, the decrease in the concentration of H defects detected above 200 °C can be described by both first and second order kinetics, with activation energies in the 1.0 eV–1.35 eV range. Further experiments on samples with different initial cluster concentrations should be performed to clearly identify the kinetics order of the defect annealing process. Taking into account the calculated frequency factors, it can be predicted that for these defects, the migration mechanism is the pathway by which they anneal-out from the silicon crystal. Based on the previously established bi-stability of the H defects and their association with a higher order of vacancy clusters as tetra-, penta-, and hexa-vacancies (V_4, V_5, and V_6), the different annealing-out behavior observed in DOFZ and STFZ silicon is attributed to their migration and reaction

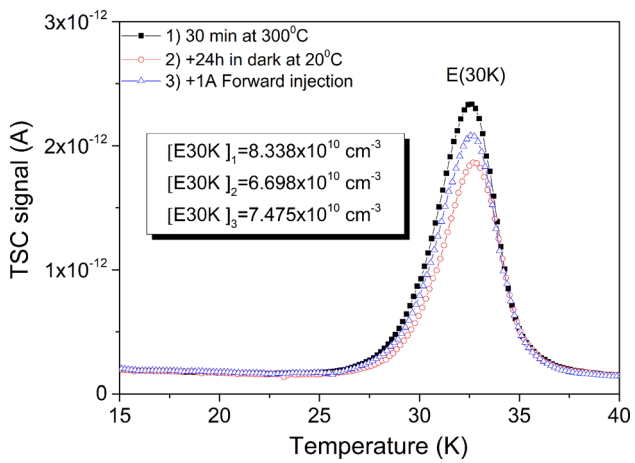

FIG. 9. Bistability of E(30 K) measured on STFZ irradiated with 3.5 MeV and a fluence of $\Phi = 6 \times 10^{14}$cm^{-2} immediately after the annealing at 300 °C, after being kept in the dark for 24 h at 20 °C and after subsequent a 4-A/cm^2 injection at 20 °C, with the filling of traps being performed at 10 K with 2 mA in all cases.

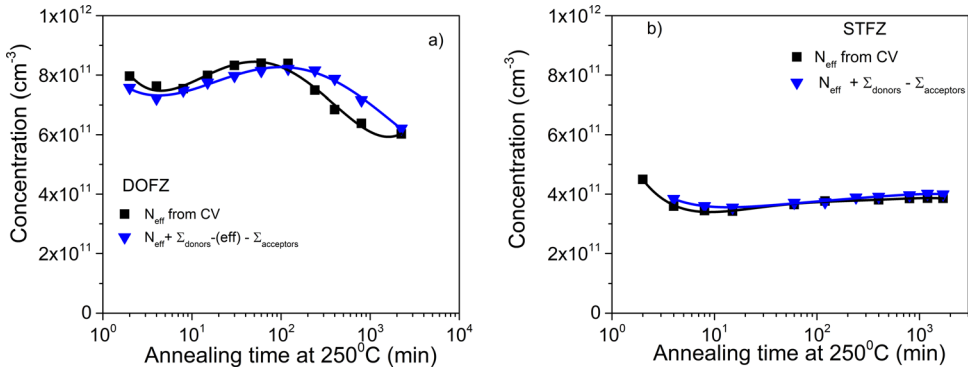

FIG. 10. The effective doping concentration, as determined from C-V characteristics at 20 °C, and the effective doping concentration calculated by accounting for all of the defects detected by TSC measurements during isothermal annealing at 250 °C on (a) DOFZ and (b) STFZ diodes irradiated with 6×10^{14} cm^{-2}.

with the oxygen present in the samples, 20 times more in DOFZ than in STFZ.

The annealing out of the E(30 K) defect takes place via a first order process with activation energy of ∼1.8 eV. The peculiar behavior of the E(30 K) donor in the two materials, that is, a 45% higher introduction rate in DOFZ silicon, indicates that the chemical structure of the defect implies oxygen. Considering only the results from the DOFZ material, where a strong decrease of the E(30 K) defect concentration is determined from the corresponding TSC spectra after annealing treatments above 200 °C, the calculated activation energy for the annealing-out process as well as the frequency factor indicates that a dissociation process takes place. However, the results on STFZ contradict such a conclusion, with the E(30 K) remaining stable up to 300 °C. Therefore, the results are explained by considering that the E(30 K) defect is bistable, and depending on the position of the Fermi level, it can switch to another configuration, most probably one that is not electrically active. Thus, new features of radiation induced cluster related defects are discussed in the present study, bringing new evidence for the impact these defects have on the performance of silicon sensors.

ACKNOWLEDGMENTS

This work has been performed in the framework of the CERN-RD50. R. Radu and I. Pintilie acknowledge the funding from the National Ministry of Research and Innovation through the Core Program and from the Romanian Authority for Scientific Research through the PCE 72/5.10.2011 Project.

[1]K. Gill, G. Hall, and B. MacEvoy, J. Appl. Phys. **82**, 126 (1997).
[2]V. P. Markevich, A. R. Peaker, S. B. Lastovskii, L. I. Murin, J. Coutinho, V. J. B. Torres, P. R. Briddon, L. Dobaczewski, E. V. Monakhov, and B. G. Svensson, Phys. Rev. B **80**, 235207 (2009).
[3]B. G. Svensson, E. V. Monakhov, G. Alfieri, M. Mikelsen, B. S. Avset, and A. Hallén, Phys. Status Solidi (c) **1**(9), 2250–2257 (2004).
[4]J. Coutinho, R. Jones, S. Öberg, and P. R. Briddond, Phys. B: Condens. Matter **340–342**, 523–527 (2003).
[5]J. Coutinho, V. P. Markevich, A. R. Peaker, B. Hamilton, S. B. Lastovskii, L. I. Murin, B. J. Svensson, M. J. Rayson, and P. R. Briddon, Phys. Rev. B **86**, 174101 (2012).
[6]B. G. Svensson and J. L. Lindström, Phys. Rev. B **34**(12), 8709 (1986).
[7]L. Fedina, A. Gutakovskii, A. Aseev, J. Van Landuyt, and J. Vanhellemont, Phys. Status Solidi (a) **171**, 147 (1999).
[8]H. Schade and D. Herrick, Solid-State Electron. **12**, 857 (1969).
[9]J. H. Bleka, L. Murin, E. V. Monakhov, B. S. Avset, and B. G. Svensson, Appl. Phys. Lett. **92**, 132102 (2008).
[10]R. Radu, I. Pintilie, L. C. Nistor, E. Fretwurst, G. Lindstroem, and L. F. Makarenko, J. Appl. Phys. **117**, 164503 (2015).
[11]I. Pintilie, E. Fretwurst, G. Lindström, and J. Stahl, Appl. Phys. Lett. **82**, 2169 (2003).
[12]I. Pintilie, E. Fretwurst, G. Lindström, and J. Stahl, Nucl. Instrum. Methods A **514**, 18 (2003).
[13]I. Pintilie, G. Lindstroem, A. Junkes, and E. Fretwurst, Nucl. Instrum. Methods A **611**, 52 (2009).
[14]A. Junkes, D. Eckstein, I. Pintilie, L. F. Makarenko, and E. Fretwurst, Nucl. Instrum. Methods A **612**, 525–529 (2010).
[15]G. Kramberger and RD50 Collaboration, Nucl. Instrum. Methods A **583**, 49 (2007).
[16]I. Pintilie, M. Buda, E. Fretwurst, G. Lindström, and J. Stahl, Nucl. Instrum. Methods A **556**(1), 197 (2006).
[17]I. Pintilie, E. Fretwurst, and G. Lindström, Appl. Phys. Lett. **92**, 024101 (2008).
[18]E. Fretwurst, F. Hönniger, G. Kramberger, G. Lindström, I. Pintilie, and R. Roder, Nucl. Instrum. Methods A **583**, 58 (2007).
[19]E. Fretwurst and RD50 Collaboration, Nucl. Instrum. Methods A **552**, 7 (2005).
[20]M. Moll and RD Collaboration, Nucl. Instrum. Methods A **546**(1-2), 99–107 (2005).
[21]G. Casse, A. Affolder, P. P. Allport, V. Chmill, D. Forshaw, A. Greenall, I. Tsurin, and T. Huse, J. Instrum. **6**, C11022 (2011).
[22]G. Kramberger and D. Contarato, Nucl. Instrum. Methods A **511**(1–2), 82 (2003).
[23]I. Mandić, V. Cindro, A. Gorišek, G. Kramberger, M. Mikuž, M. Milovanović, and M. Zavrtanik, J. Instrum. **8**, P04016 (2013).
[24]J. Lange, M. C. Areste, E. Cavallaro, F. Förster, S. Grinstein, I. L. Paz, M. Manna, G. Pellegrini, D. Quirion, S. Terzo, and D. Vázquez Furelos, J. Instrum. **11**, C11024 (2016).
[25]See www.hilumilhc.web.cern.ch for information about the High Luminosity LHC.
[26]See www.rd50.web.cern.ch for information about research and development of radiation hard semiconductor devices for very high luminosity colliders.
[27]B. T. Huffmana and ATLAS Collaboration, in Proceedings for IPRD13, Italy (2013).
[28]M. Huhtinen, Nucl. Instrum. Methods Phys. Res. A **491**, 194 (2002).
[29]J. Zhang, I. Pintilie, E. Fretwurst, R. Klanner, H. Perrey, and J. Schwandt, J. Synchrotron Radiat. **19**, 340–346 (2012).
[30]G. D. Watkins and J. W. Corbett, Phys. Rev. **121**(4), 1001 (1961).
[31]G. D. Watkins, *Radiation Damage in Semiconductors* (Dunod, Paris, 1965), p. 97.
[32]J. W. Corbett and G. D. Watkins, Phys. Rev. Lett. **7**(8), 314 (1961).
[33]A. V. Dvurechenskii and A. A. Karanovich, Sov. Phys. Semicond. **19**(11), 1198 (1985).
[34]Y. H. Lee and J. W. Corbett, Phys. Rev. B **13**(6), 2653 (1976).
[35]See www.cismst.org for information about CiS Reasearch Institute for Micro Sensors and Photovoltaics GmbH, 99099, Erfurt, Germany.
[36]See www.bsu.by for information about Belarusian State University.
[37]A. Barcz, M. Zielinski, E. Nossarzewska, and G. Lindström, Appl. Surf. Sci. **203–204**, 396 (2003).

[38]I. Pintilie, L. Pintilie, M. Moll, E. Fretwurst, and G. Lindstroem, Appl. Phys. Lett. **78**(4), 550–552 (2001).
[39]J. Bourgoin and M. Lannoo, *Point Defects in Semiconductors II Experimental Aspects* (Springer-Verlag, Berlin, Heidelberg/New York, 1983). ISBN-13:978-3-642-81834-9.
[40]B. Surma, P. Kamiński, A. Wnuk, and R. Kozłowski, "Optical studies of defect centers formed in MCz-Si and FZ-Si by high fluence neutron irradiation," in 17th RD50 Workshop, Geneva, 17–19 November 2010.
[41]E. Donegani, "Energy-dependent proton damage in silicon," Report No. DESY-THESIS-2017-042, Hamburg (2017).
[42]D. V. Makhov and L. J. Lewis, Phys. Rev. Lett. **92**, 255504 (2004).
[43]T. E. M. Staab, A. Sieck, M. Haugk, M. J. Puska, Th. Frauenheim, and H. S. Leipner, Phys. Rev. B. **65**, 115210 (2002).
[44]M. Mikelsen, E. V. Monakhov, G. Alfieri, B. S. Avset, and B. G. Svensson, Phys. Rev. B **72**, 195207 (2005).
[45]M. Mikelsen, J. H. Bleka, J. S. Christensen, E. V. Monakhov, B. G. Svensson, J. Härkönen, and B. S. Avset, Phys. Rev. B **75**, 155202 (2007).
[46]V. P. Markevich, A. R. Peaker, B. Hamilton, S. B. Lastovskii, L. I. Murin, J. Coutinho, V. J. B. Torres, L. Dobaczewski, and B. G. Svensson, Phys. Status Solidi (a) **208**, 568–571 (2011).
[47]S. K. Estreicher, Phys. Status Solidi (b) **217**, 513 (2000).
[48]I. Pintilie, M. Buda, E. Fretwurst, F. Hönniger, G. Lindström, and J. Stahl, Nucl. Instrum. Methods A **552**, 56–60 (2005).